

Geophysical Research Letters

RESEARCH LETTER

10.1029/2020GL091103

Key Points:

- New methodology to examine the Southern Ocean response to climate extremes using perturbation simulations with realistic atmospheric forcing
- Southern Ocean overturning circulation exhibits a rapid response that is sustained in depth-latitude space but decays in density-latitude space
- Adjustment of the ocean interior occurs along isopycnals at a rate of order 1° latitude per year, depending of the representation of eddies

Supporting Information:

- Supporting Information S1

Correspondence to:

K. D. Stewart,
kial.stewart@anu.edu.au

Citation:

Stewart, K. D., Hogg, A. M., England, M. H., & Waugh, D. W. (2020). Response of the Southern Ocean overturning circulation to extreme Southern Annular Mode conditions. *Geophysical Research Letters*, 47, e2020GL091103. <https://doi.org/10.1029/2020GL091103>

Received 5 OCT 2020

Accepted 25 OCT 2020

Accepted article online 2 NOV 2020

Response of the Southern Ocean Overturning Circulation to Extreme Southern Annular Mode Conditions

K. D. Stewart^{1,2} , A. McC. Hogg^{1,3} , M. H. England^{2,3} , and D. W. Waugh^{4,5} 

¹Research School of Earth Sciences, Australian National University, Canberra, ACT, Australia, ²Climate Change Research Centre, University of New South Wales, Sydney, New South Wales, Australia, ³Australian Research Council Centre of Excellence for Climate Extremes, Canberra, ACT, Australia, ⁴Department of Earth and Planetary Sciences, The Johns Hopkins University, Baltimore, MD, USA, ⁵School of Mathematics and Statistics, University of New South Wales, Sydney, New South Wales, Australia

Abstract The positive trend of the Southern Annular Mode (SAM) will impact the Southern Ocean's role in Earth's climate; however, the details of the Southern Ocean's response remain uncertain. We introduce a methodology to examine the influence of SAM on the Southern Ocean and apply this method to a global ocean-sea ice model run at three resolutions (1° , $(1/4)^\circ$, and $(1/10)^\circ$). Our methodology drives perturbation simulations with realistic atmospheric forcing of extreme SAM conditions. The thermal response agrees with previous studies; positive SAM perturbations warm the upper ocean north of the wind speed maximum and cool it to the south, with the opposite response for negative SAM. The overturning circulation exhibits a rapid response that increases/decreases for positive/negative SAM perturbations and is insensitive to model resolution. The longer-term adjustment of the overturning circulation, however, depends on the representation of eddies, and is faster at higher resolutions.

Plain Language Summary The Southern Ocean has accounted for the vast majority of the global ocean heat uptake since the early 2000s. The atmospheric winds over the Southern Ocean play a leading role in its ability to uptake heat, by way of driving much of the Southern Ocean circulation. Observations of these winds indicate that they have been steadily changing over the past few decades, and hence, so too is the Southern Ocean heat uptake. However, despite recent research efforts, the details of the Southern Ocean's response to these changing winds remain uncertain. Here we introduce a novel methodology to examine the Southern Ocean's response to changing winds. We perform numerical simulations with a global ocean-sea ice model suite that spans a hierarchy of spatial resolutions and driven by realistic atmospheric forcing conditions. The initial response of the Southern Ocean circulation to changes in winds is robust across the model suite and insensitive to model resolution; longer-term response, however, depends on the representation of eddies in the model.

1. Introduction

The Southern Ocean has accounted for between 67% and 98% of the total ocean heat uptake since 2005 (Llovel & Terray, 2016; Roemmich et al., 2015). This Southern Ocean heat uptake, which is predominantly in the upper 2 km, results from the intricate interplay between surface fluxes of heat and momentum, ocean circulation, and the associated redistribution of existing oceanic heat reservoirs (Armour et al., 2016; Frölicher et al., 2015; Marshall et al., 2015). Southern Hemisphere winds play a leading role in these proposed mechanisms of Southern Ocean heat uptake. It follows that Southern Ocean heat uptake, and thus global ocean warming, will be sensitive to processes that govern Southern Hemisphere winds.

The Southern Annular Mode (SAM) is the primary mode of climate variability in the extratropical Southern Hemisphere (Thompson & Wallace 2000; Thompson, Wallace & Hegerl 2000). The SAM dynamically influences the strength and latitudinal location of the Southern Hemisphere midlatitude westerly winds. Following Gong and Wang (1999), the SAM can be characterized by a SAM index based on the normalized monthly zonal mean sea level pressure difference between 40°S and 65°S . Observations indicate there has been a positive trend in the SAM index since the 1950s (Marshall, 2003; Thompson & Solomon, 2002), which is projected to continue due to anthropogenic forcing (Zheng et al., 2013). It is anticipated that this

trend in the SAM index, and the associated trends in the strength and position of the Southern Hemisphere midlatitude westerly winds, will influence Southern Ocean warming (e.g., Armour et al., 2016).

Examining the influence of the SAM on the Southern Ocean often employs regression and/or correlation analysis techniques, instantaneous or time lagged, to ascribe changes in the ocean state with the value of the SAM index. This approach is particularly useful for studies that use satellite- or Argo-based observations, coupled climate model output, or reanalysis products (e.g., Hazel & Stewart, 2019; Kosempa & Chambers, 2014; Lovenduski & Gruber, 2005; Sen Gupta & England, 2006). Another approach is to examine composites of ocean states based on SAM index thresholds to average out signals that are not SAM related (e.g., Li et al., 2019; Sallée et al., 2010). Such methodologies are convenient since the independent variable (the SAM index) is unable to be controlled in these data sets; however, the transient response of the system may act to obscure correlations. These approaches demonstrate that of all the atmospheric variability associated with the SAM, the Southern Ocean is most sensitive to the SAM-related changes in wind forcing (e.g., Sen Gupta & England, 2006).

An alternative approach to understand the influence of SAM in the Southern Ocean uses perturbation simulations. Given that the Southern Ocean is most sensitive to the wind changes associated with SAM, these simulations typically consist of an extended duration control run driven by repeating year forcing, from which perturbation runs are branched. These perturbation simulations have some idealized modification of their wind forcing fields stylized on the SAM associated strengthening and/or poleward shifting of the Southern Hemisphere midlatitude westerly winds (e.g., Farneti, Delworth, Rosati et al., 2010; Gent & Danabasoglu, 2011; Hofmann & Morales-Maqueda, 2011; Spence et al., 2014; Waugh et al., 2019). Note that the focus of these SAM-influenced perturbation studies has been to understand the response of the Southern Ocean to the observed positive trend in the SAM, and as such they generally do not impose forcing anomalies representative of negative SAM conditions. Nevertheless, this approach has the advantage, and disadvantage, that the idealized wind anomalies can be manipulated in time, space, structure and magnitude, such that the permutations of the anomaly configuration are without limit. Given the multitude of anomaly permutations, a sensible approach is to keep the anomaly configuration as simple as possible, which begs the question: Is the Southern Ocean response fundamentally different if *any* complexity is added to the anomaly? Another important consideration for such experiments is that the idealized wind anomalies are typically applied without regard to other aspects of the climate that then become physically inconsistent. For instance, a real poleward shifting of the wind field would be accompanied by a shift of the storm tracks, as well as the cloud cover and air temperatures; these forcing fields typically remain unmodified in the perturbation simulations.

Here we introduce a new methodology to simulate and examine the influence of SAM on the Southern Ocean in a global ocean-sea-ice model that uses realistic, reanalysis based, repeating year atmospheric forcing to drive both control and SAM perturbation simulations. For the control forcing, the repeating year is a period of climatologically neutral conditions; for the perturbations, the repeating years are periods of both extreme positive and extreme negative SAM conditions. While this approach brings an increased level of complexity to the dynamical structure of the perturbation, it greatly reduces the subjectivity of the perturbation configuration and maintains the physical consistency of its forcing fields. This methodology is described in section 2, and the thermal response of the Southern Ocean to the extreme SAM forcing conditions is presented in section 3. We then compare the response of the Southern Ocean overturning circulation to the extreme SAM forcing conditions, examining the overturning in both depth-latitude and density-latitude coordinates (section 4). Finally section 5 covers the summary of our results and conclusions.

2. Model and Methodology

We employ the Australian Community Climate and Earth System Simulator, ocean-sea-ice model Version 2 (ACCESS-OM2; Kiss et al., 2020), a modeling suite developed by the Consortium for Ocean-Sea-Ice Modelling in Australia (COSIMA), to simulate the global ocean-sea-ice response to changes in imposed atmospheric conditions. This suite includes global ocean-sea-ice model configurations with horizontal grid spacings of nominally 1° (ACCESS-OM2), 0.25° (ACCESS-OM2-025), and 0.1° (ACCESS-OM2-01) latitude and longitude; here we use all three configurations. Following Stewart et al. (2017), the grid spacings of the generalized z^* vertical coordinate of the ocean models are objectively constructed to support the vertical structure of the baroclinic dynamics permitted by the horizontal grids.

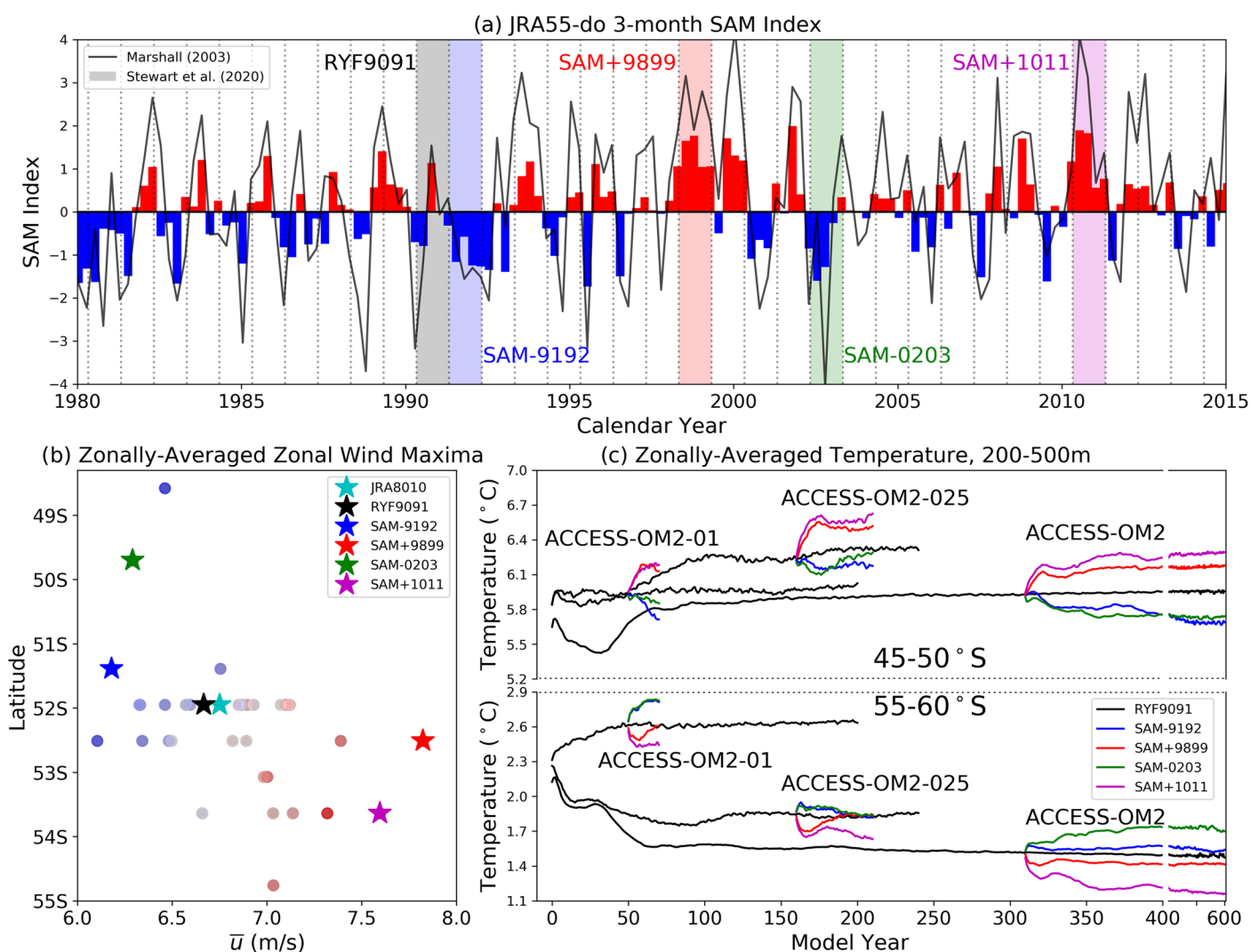


Figure 1. (a) Three-monthly SAM index calculated from the JRA55-do data set. The RYF9091 and four SAMx periods are shaded. For comparison, the equivalent observational station-based SAM index of Marshall (2003) is included in black. (b) The zonally averaged zonal wind maximum speed and latitudinal locations for the RYF9091 and SAMx periods. Also included is the 1980–2010 average of the JRA55-do data set (JRA8010; cyan star) as a climatological reference, and all remaining May–April periods between 1980–2015 colored blue-red by their respective SAM index (dots). (c) Time series of the simulated zonally averaged temperatures between 200–500 m depth for 45–50°S (upper) and 55–60°S (lower); these latitudinal bands are selected to lie either side of the zonal wind speed maxima.

The two coarser configurations implement the Gent and McWilliams (1990) (GM) parameterization to represent underresolved mesoscale eddies with an associated diffusivity that is flow-dependent (see Griffies et al., 2005) and scaled by the ability of the horizontal grid to resolve the first baroclinic Rossby radius (as per Hallberg, 2013), and the Redi (1982) parameterization for along-isopycnal diffusion with a coefficient of $600 \text{ m}^2/\text{s}$ for ACCESS-OM2 and up to $200 \text{ m}^2/\text{s}$ for ACCESS-OM2-025 (scaled by the local grid resolution and Rossby radius). For further details and evaluation of the ACCESS-OM2 suite see Kiss et al. (2020).

The ACCESS-OM2 simulations are initialized with January temperature and salinity fields from the World Ocean Atlas 2013 (WOA13; Locarnini et al., 2013; Zweng et al., 2013). The simulations are forced with prescribed atmospheric conditions taken from the high-resolution, self-consistent Japanese atmospheric reanalysis data set for driving ocean models (JRA55-do; Tsujino et al., 2018). These prescribed atmospheric conditions, described in detail by Stewart et al. (2020), are the 12-month period from 1 May 1990 to 30 April 1991 used repeatedly to drive the simulations. In practice, the forcing runs from 1 January 1991 to 31 December 1990 with a sudden transition from 30 April 1991 back to 1 May 1990; shifting the sudden

transition away from the December solstice reduces the intensity of weather variability at the time of transition. This repeated year forcing period, referred to as RYF9091, has been identified as a quasi-climatological period of the JRA55-do data set with neutral values of all major climate indices, including the SAM index (see Figure 1a). These RYF9091 simulations have two primary purposes; they provide for an extended period of model adjustment from the WOA13 state over which the model drift can be assessed, and they serve as control simulations from which perturbation simulations can be branched and compared.

A further four forcing periods are identified from the JRA55-do record; these are 12-month periods, running 1 May to 30 April of the following year, with anomalous (positive and negative) SAM conditions, collectively referred to as SAMx periods. The extreme negative SAMx periods (SAM– years) are 1991–1992 and 2002–2003, and the extreme positive SAMx periods (SAM+ years) are 1998–1999 and 2010–2011 (Figure 1a); these periods are referred to as SAM–9192, SAM–0203, SAM+9899, and SAM+1011, respectively, and are used to drive perturbation simulations branched from the RYF9091 control simulations. The annual averages of the zonally averaged zonal winds of the SAMx periods are shown in Figure 1b; the relationship between the SAM index and the wind speed strength and latitudinal distribution is evident, as well as the degree to which our identified SAMx periods are extreme. For reference, the relative differences in the zonally averaged zonal winds between the SAMx and RYF9091 periods are distinct for the SAM+ and SAM– cases and reach +30% for the SAM+ and –15% for the SAM– periods. While these large changes in the wind fields dominate the atmospheric signature of extreme SAM periods, our technique has the advantage that synchronous changes in other fields (including the buoyancy forcing) are naturally included. Additionally, the respective increase or decrease of the wind speed maxima for a given SAMx forcing period is mirrored northwards of $\sim 45^{\circ}$ S, such that, for instance, the zonal wind speed of the SAM+ periods is less than the JRA55-do climatological mean; this is a forcing feature that is typically not included in experiments with idealized wind perturbations (e.g., Spence et al., 2014).

The RYF9091 control simulations are initialized from rest with the WOA13 hydrography and run for 600, 240, and 200 years for the 1° , 0.25° , and 0.1° model configurations, respectively. Following an initial adjustment period (310, 160, and 50 years for the 1° , 0.25° , and 0.1° model configurations, respectively; Figure 1c), simulations with the SAMx forcing conditions are branched off and run alongside the control simulations for 290, 50, and 20 years for the 1° , 0.25° , and 0.1° model configurations, respectively. This methodology allows for the direct comparison of the perturbation-control differences across the suite of model configurations. While the primary focus of the analysis here is the response of the Southern Ocean overturning circulation, to begin with we briefly examine the zonally averaged thermal responses.

3. Thermal Response

The initial response of the upper Southern Ocean temperature to the sudden change in forcing is consistent with previous studies (e.g., Gent & Danabasoglu, 2011); north of the zonal wind speed maximum the upper ocean temperatures increase for SAM+ perturbations (and decreases for SAM– perturbations) by approximately 0.2°C within 5 years, with the opposite response occurring south of the zonal wind speed maximum (Figure 1c). The magnitude and timescale of these initial responses are distinct from the gradual temperature changes arising from model drift, and insensitive to model resolution. Following an initial adjustment period, these thermal responses are either sustained for the duration of the perturbation simulations, or trend back towards the respective RYF9091 simulation; importantly, they do not continue to grow with time.

Figures 2a–2d depicts the depth-latitude distributions of the zonally averaged temperature anomalies for the (a, b) SAM+9899 and (c, d) SAM–0203 forced ACCESS-OM2-01 simulations, averaged for the (a, c) third and (b, d) ninth years after the perturbation. The SAM+9899 perturbation exhibits thermal anomaly distributions that are consistent with the south-north cooling-warming response straddling the wind speed maximum previously described by Sen Gupta and England (2006). The thermal response of the SAM–0203 perturbation exhibits relatively more structure, but of reduced intensity compared to the SAM+9899 response. Equivalent temperature anomaly distributions for the SAM+1011 and SAM–9192 simulations are presented in Figure S1 in the supporting information; the comparison of these figures highlights the consistent thermal response of the respective SAM+ and SAM– cases, particularly south of 30° S for SAM+ and 40° S for SAM–. All cases exhibit local extrema in the thermal responses at around 800–900 m depth; for SAM+ this occurs between 35° S and 45° S, and for SAM– between 40° S and 50° S. Comparing the thermal

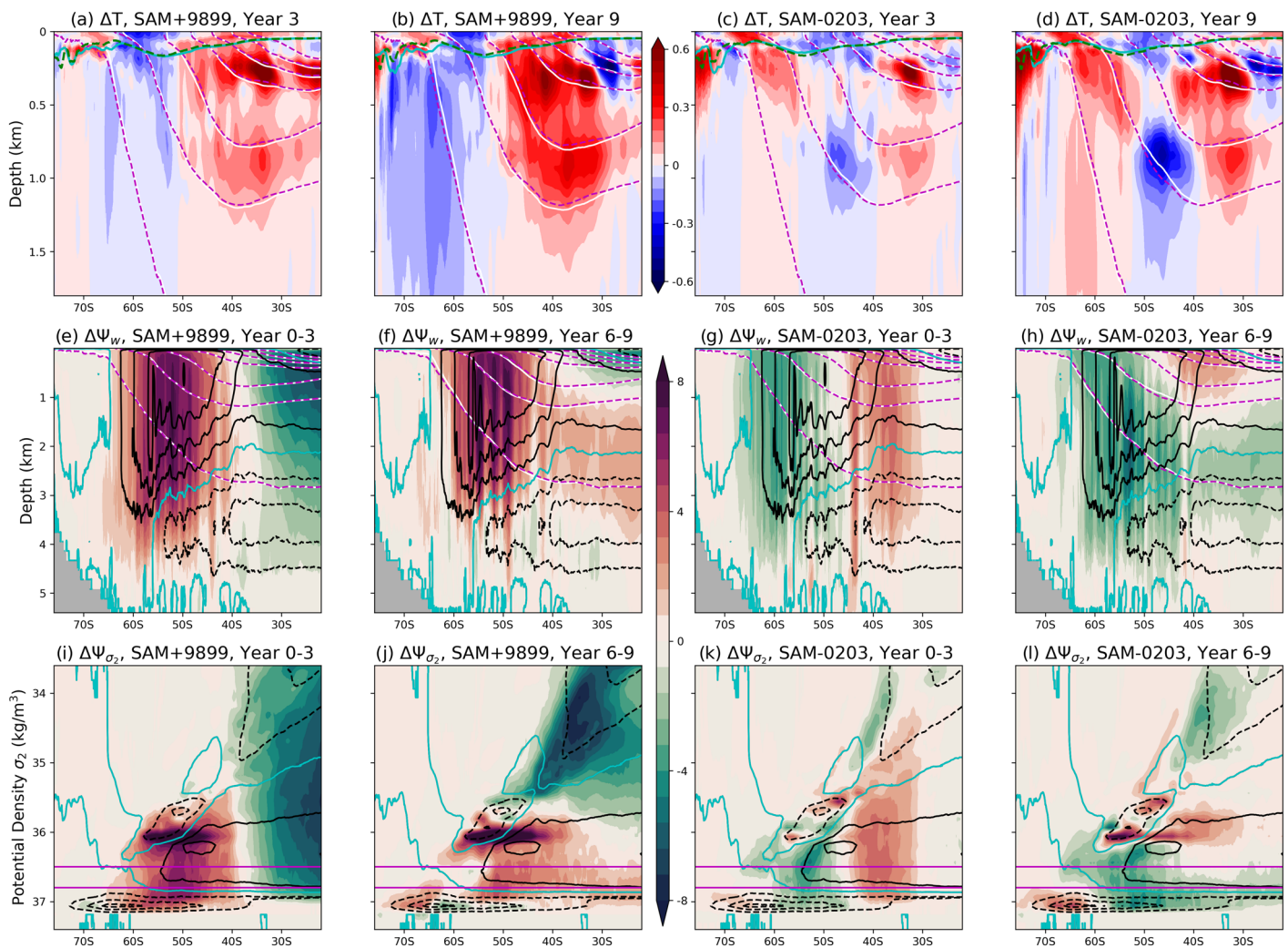


Figure 2. (a–d) Distributions of the Year 3 (a, c) and 9 (b, d) temperature anomalies from the 0.1° ACCESS-OM2-01 for (a, b) SAM+9899 and (c, d) SAM–0203 simulations. The white and dashed magenta contours represent the SAMx and RYF9091 isopycnals at $\sigma_2 = 0.5 \text{ kg/m}^3$ intervals, respectively, spanning $\sigma_2 = 34\text{--}37 \text{ kg/m}^3$ inclusive, with the cyan and dashed green contours representing the respective mixed-layer depths. (e–h) The w stream function anomalies of the ACCESS-OM2-01 simulations with SAM+9899 (e, f) and SAM–0203 (g, h) averaged for the Years 0–3 (e, g) and 6–9 (f, h). Contoured in black is the Ψ_w for the RYF9091 case at $\pm 7.5 \text{ Sv}$ intervals with the 0 Sv contour in cyan. The white and dashed magenta contours represent the same isopycnals as in (a)–(d). Panels (i)–(l) depict a similar analysis to panels (e)–(h) but for the σ_2 stream function anomalies. The magenta lines in (i)–(l) at 36.5 and 36.8 kg/m^3 indicate the regions of interest for Figure 3.

anomaly distributions for the Year 3 and Year 9 responses shows that, while the thermal responses intensify in time, they retain their initial structure.

The zonally averaged temperature anomalies are composed of a combination of processes which include the wind-driven movement of isopycnals, defined as “heave” by Bindoff and McDougall (1994), and the change of temperature on isopycnals due to changes of along isopycnal transport and stirring. In the figures of zonally averaged temperature anomaly, heave is evidenced by the spatial correlation between the vertical displacement of isopycnals and the sign of the thermal anomalies. The diagnosed contributions from heave and the change of temperature on isopycnals for the SAM+9899 and SAM–0203 cases at all three model resolutions are shown in Figure S2. The contribution from heave is insensitive to model resolution, which is perhaps to be expected as to leading order heave is a wind-driven process. Heave is strongest north of 50°S and accounts for the local extrema in the thermal responses around 800–900 m depth. The contribution from temperature changes on isopycnals, however, is surface intensified, strongest south of 50°S , and resolution dependent; this distribution makes sense considering the important role that eddies play in along isopycnal stirring and transport. Time series of these contributions to the thermal anomalies north and south of

the wind speed maxima show the longer-term thermal responses (Figure S3); importantly, the SAM+ and SAM– perturbations are distinct in all cases. South of the wind speed maxima, the change of temperature on isopycnals dominates over the heave-associated response and strengthens with refined model resolution. North of the wind speed maxima, however, the heave and isopycnal temperature changes have contributions of similar magnitude and appears insensitive to model resolution.

4. Overturning Circulation Response

Considering the rapid timescale of thermal adjustment, the initial dominance of heave, and the structure of the thermal anomalies relative to the wind speed maxima, the thermal response indicates a wind-driven modification of the Southern Ocean overturning circulation. To examine the response of the overturning circulation, we evaluate and compare two overturning stream functions independently diagnosed from the simulations. Following Zika et al. (2012), the first stream function Ψ_w (m^2/s) is derived by integrating the vertical velocity in longitude and northward from the Antarctic coastline up to a given latitude y , that is,

$$\Psi_w(y, z, t) = \int_{90^\circ S}^y \int w(x, y', z, t) dx dy', \quad (1)$$

where w is the annually averaged vertical velocity, giving Ψ_w in depth-latitude-time coordinates. Taking σ_2 as the potential density of seawater referenced to 2,000 dbar less 1,000 kg/m^3 , a second overturning stream function Ψ_{σ_2} (m^2/s) can be diagnosed by integrating the along-isopycnal meridional velocity in longitude and from the densest isopycnal class ($\sigma_2 > 38$) to a given isopycnal σ_2 , as

$$\Psi_{\sigma_2}(y, \sigma_2, t) = \int_{38}^{\sigma_2} \int v_{\sigma_2}(x, y, \sigma'_2, t) dx d\sigma'_2, \quad (2)$$

where v_{σ_2} is the along-isopycnal meridional velocity, returning Ψ_{σ_2} in density-latitude-time coordinates. We refer to these two overturning stream functions as the w stream function and σ_2 stream function, respectively.

The depth-latitude distributions of $\Delta\Psi_w$ for the ACCESS-OM2-01 cases of SAM+9899 and SAM–0203 are shown in Figures 2e–2h; these are 3-year averages for the Years 0–3 (e, g) and 6–9 (f, h). The initial responses of $\Delta\Psi_w$ are seemingly depth-independent above $\sim 3,000$ m. In time, the w stream function anomalies equatorward of 40–45°S develops vertical structure that appears to propagate along isopycnals; note that the Ψ_w anomalies poleward of 40–45°S maintain their initial structure and intensity. For the SAM+ cases, the structure, magnitude, and evolution of the Ψ_w response is similar to that of the high-resolution simulations reported in previous studies (e.g., Farneti & Delworth 2010); however, we do not find the Ψ_w response to be resolution dependent. Given the implementation of a variable, flow-dependent GM diffusivity in the ACCESS-OM2 simulations at coarser resolutions, this insensitivity of the Southern Ocean response to the model resolution is indeed to be expected (Gent, 2016).

The interior structure of the time evolution of these overturning circulation responses is more apparent in the σ_2 stream function anomalies (Figures 2i–2l). The Years 0–3 $\Delta\Psi_{\sigma_2}$ anomalies depend primarily on latitude for densities greater than $\sim 35.5 \text{ kg}/\text{m}^3$. By Years 6–9 these anomalies have become more dependent on density and less dependent on latitude. The structure of the longer-term distributions of $\Delta\Psi_{\sigma_2}$, especially south of 40°S, tends to align with isopycnals and appears to propagate northward.

The progression of the Ψ_{σ_2} anomalies into the interior along isopycnal pathways can be seen in time-latitude Hovmöller diagrams, for which we use the mean of the σ_2 range 36.5–36.8 kg/m^3 (Figure 3). The initial responses of all perturbations are insensitive to the model resolutions used here, and are characterized by regions of opposite signed signals either side of ~ 40 –45°S. In time, the equatorward signal diminishes, and in the cases of SAM+9899 and SAM–9192, vanishes within 5–8 years. For the SAM+ simulations with ACCESS-OM2-01, the boundary separating the opposite signed signals is observed to propagate equatorward at a rate of order 1° of latitude per year (dashed black lines in Figure 3). For reference, this rate of propagation corresponds to an along-isopycnal diffusion with a coefficient of 390 m^2/s . The latitudinal progression of this signal represents the adiabatic, along-isopycnal propagation of a wind forcing perturbation into the ocean interior (e.g., Doddridge et al., 2016). That is, the perturbation of the wind field initially excites an Eulerian response that is largely barotropic in nature and with the same latitudinal structure as the wind perturbation (Figures 2e and 2g); in time, this initial Eulerian response penetrates equatorward into the ocean interior,

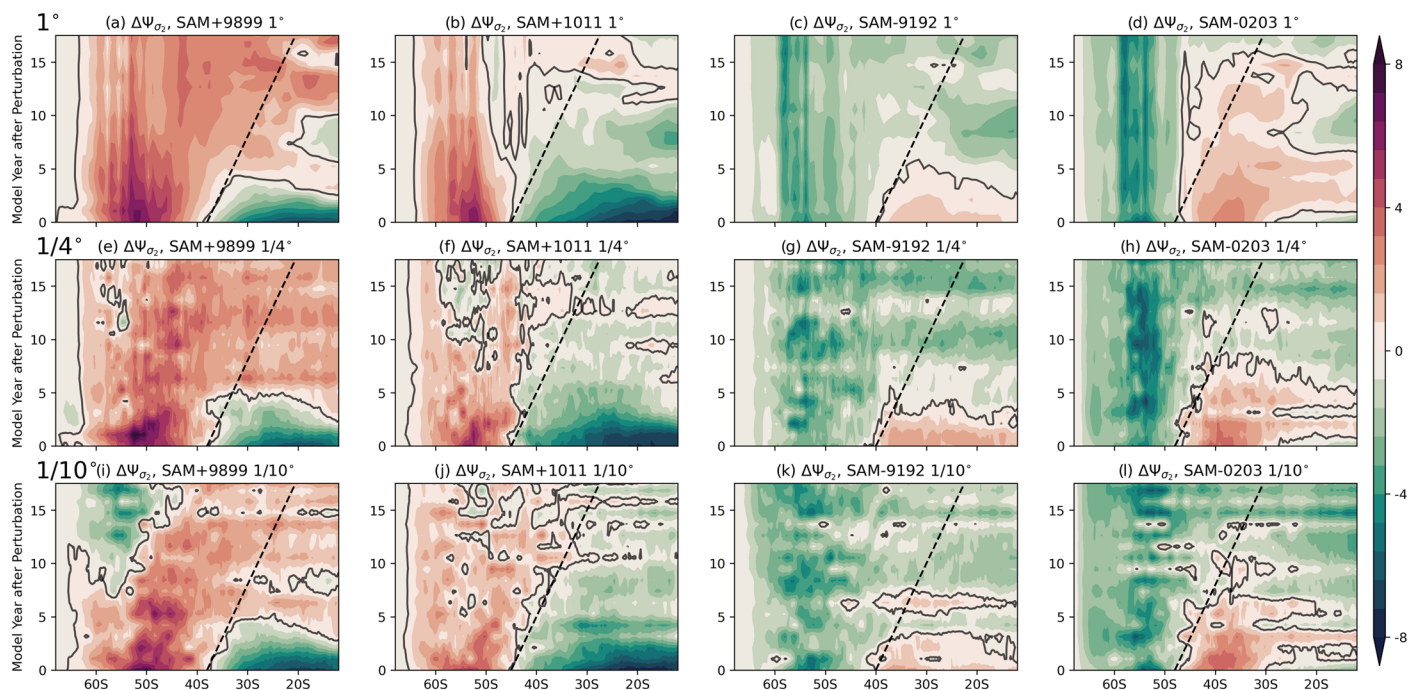


Figure 3. Hovmöller diagrams of the σ_2 stream function anomalies for the (a, e, and i) SAM+9899, (b, f, and j) SAM+1011, (c, g, and k) SAM-9192, and (d, h, and l) SAM-0203 cases and the 1° , $(1/4)^\circ$, and $(1/10)^\circ$ simulations (rows top-to-bottom, respectively). The $\Delta\Psi_{\sigma_2}$ is calculated as the 36.5 – 36.8 kg m^{-3} average, as indicated in Figures 2i–2l. The $\Delta\Psi_{\sigma_2} = 0 \text{ Sv}$ contour is included for reference, as well as the dashed slope which represents an along-isopycnal velocity of 1° latitude per year.

predominantly adiabatically along isopycnals, a process that is likely dependent on eddies (parameterized or resolved), and hence model resolution. This demonstration of the initial and time-evolving adjustments reflects the multiple timescale responses that can arise from changes in atmospheric forcing over the Southern Ocean (e.g., Armour et al., 2016; Waugh & Haine, 2020).

An additional measure of the Southern Ocean overturning circulation response can be found by comparing the 24-month mean maxima of Ψ_w and Ψ_{σ_2} for the region of interest (south of 30°S). In the case of Ψ_w , the Southern Ocean maximum represents the strength of the “Deacon cell,” a localized wind-driven overturning of waters in Eulerian space with near-uniform properties such that it is unable to substantially contribute to the meridional transport of tracer (e.g., Zika et al., 2012). Figures 4a–4c shows the Southern Ocean maximum of Ψ_w increases for SAM+ and decreases for SAM– perturbations and that this response does not evolve in time. This immediate and sustained response of the Ψ_w overturning stream function is consistent with the findings of Treguier et al. (2010), who report a high correlation ($r = 0.79$) between the Southern Ocean mean flow overturning and the SAM index in a global ocean-sea-ice simulation driven by atmospheric forcing with interannual variability.

The Southern Ocean maximum of Ψ_{σ_2} (Figures 4d–4f), however, initially exhibits a response that is of similar magnitude to the respective Ψ_w response but is time dependent. The magnitude of the initial Ψ_{σ_2} maxima anomalies decreases as the model resolution is refined (compare the initial differences between the Ψ_{σ_2} maxima of SAMx and RYF9091 across the resolutions). For the SAM+ cases, the Ψ_{σ_2} maxima decays back toward the RYF9091 value with an adjustment timescale of approximately a decade for the 0.1° resolution case, and longer for the coarser resolutions. The Ψ_{σ_2} maxima of the SAM– cases are initially less than that of the RYF9091 and appear to continue decreasing for the first two decades; the longer, coarser resolution simulations suggest these Ψ_{σ_2} values stabilize for a couple of decades before returning toward the RYF9091 level. The initial response of the Ψ_{σ_2} is consistent with the results of Farneti et al. (2015), who found the correlation between the Southern Ocean upper cell overturning in density space and the SAM index of a multimodel ensemble to be high ($r = 0.67$), but not as high as that of Treguier et al. (2010) for the mean flow overturning. Farneti et al. (2015) also report that the Ψ_{σ_2} -SAM correlations of their various models are weaker for models with more responsive eddy fluxes ($r = 0.56$), and stronger for models with less responsive eddy fluxes

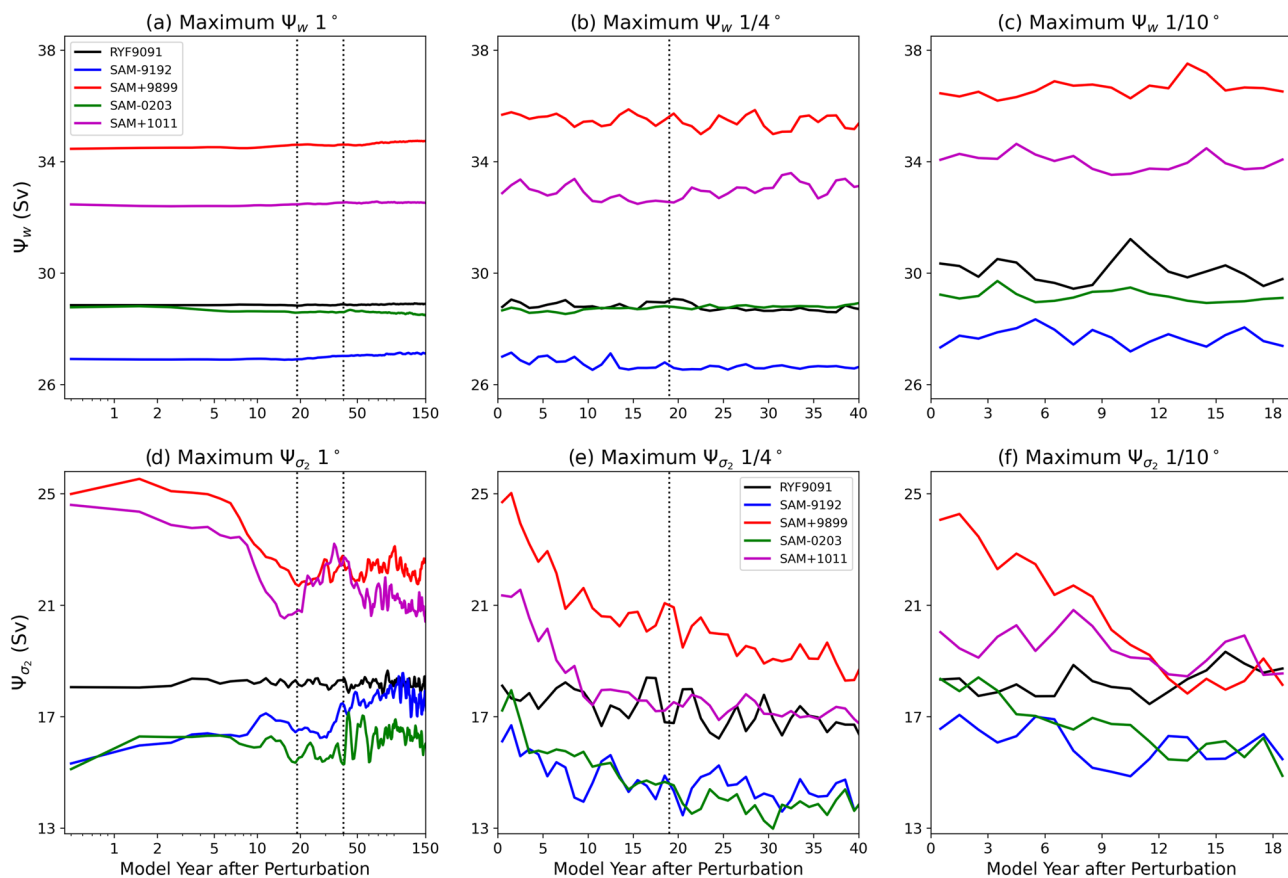


Figure 4. Time series of the maximum 24-month mean Ψ_w (a–c) and Ψ_{σ_2} (d–f). Note the different time axes for different resolutions (columns); the vertical dotted lines in the ACCESS-OM2 and ACCESS-OM2-025 plots indicate the extent of the time series of the higher-resolution panels.

($r = 0.82$). In the context of our findings of the time-dependent Ψ_{σ_2} response, a stronger rate of decay, indicative of a weakening of the Ψ_{σ_2} -SAM correlation, can be interpreted as more responsive eddy fluxes, with the timescale of adjustment being set by the spin-up time of the eddy field. This interpretation is consistent with the increased initial Ψ_{σ_2} response for the coarser resolution simulations.

The results presented here demonstrate that the response of the Southern Ocean overturning circulation to sudden and extreme perturbations of SAM conditions is composed of the following:

- a rapid and sustained adjustment of the wind-driven Deacon cell, represented here as Ψ_w , that increases for SAM+ and decreases for SAM- perturbations and is insensitive to model resolution; and
- an initial adjustment of the density-latitude overturning circulation, Ψ_{σ_2} , that is comparable to that of Ψ_w but subsequently decays in time at a rate that depends on model resolution.

This analysis portrays the process by which the initial overturning response is ingested into the ocean interior; that is, adiabatically along isopycnals, which for the high-resolution simulations with SAM+ perturbations occurs at a rate of order 1° latitude per year.

5. Conclusion

We have presented a novel methodology for perturbing global ocean-sea-ice models driven by prescribed atmospheric forcing. Here, this methodology employs periods of extreme SAM conditions identified in the JRA55-do data set to branch perturbation simulations from a control. By using periods of extreme yet realistic atmospheric conditions, as opposed to idealized modifications of control conditions, we maintain the physical fidelity of the JRA55-do forcing across its fields. This approach provides confidence that the magnitude of the forcing perturbation is climatologically relevant, even if the timescale of the forcing perturbation

is not. The focus here is on extreme SAM conditions, however, this methodology could be used to examine the ocean-sea-ice response to other major climate indices.

The analysis of the perturbation simulations demonstrates the utility of the new methodology for examining the response of the Southern Ocean to extreme SAM forcing conditions. The thermal response to the perturbed forcing, especially the contribution from isopycnal heave, is insensitive to the model resolutions used here; the exception to this is the change of temperature on isopycnals, which intensifies as model resolution is refined, reflecting the important role of eddies in this process. The response of the Southern Ocean overturning circulation to extreme SAM conditions consists of a rapid and sustained adjustment of the wind-driven Deacon cell, and an initial adjustment of the density-latitude overturning circulation that decays in time. The overturning circulation responses are found to project into the interior, propagating northward along isopycnals at a rate of order 1° of latitude per year. It is argued that the adjustment of the overturning in density-latitude coordinates represents the spin-up of the adiabatic eddy field in response to the extreme SAM forcing conditions. Finally, considering the continued strengthening trend of the SAM in the present-day climate, we can anticipate associated increases in the Southern Ocean overturning circulation in depth-latitude coordinates, and an ongoing adjustment of the overturning in density-latitude coordinates and Southern Ocean eddy field.

Data Availability Statement

The ACCESS-OM2 model output is in the process of being uploaded to the COSIMA Model Output Collection; when this process is complete the data will be available online (<https://doi.org/10.4225/41/5a2dc8543105a>).

Acknowledgments

We acknowledge the support of this work from the Earth Systems and Climate Change Hub funded by the Australian Government's National Environmental Science Program (NESP). Many thanks to Navid Constantinou, Ryan Holmes, Qian Li, Adele Morrison, and Jan Zika for very helpful discussions, and to the COSIMA consortium (www.cosima.org.au) for making available the ACCESS-OM2 suite of models. We also thank Chris Chapman who proposed the idea of the repeating year extreme SAM perturbation experiments at the Australian Research Council Centre of Excellence for Climate Extremes 2018 SAM workshop. The numerical simulations and analysis were performed with the resources of the National Computational Infrastructure (Canberra, Australia).

References

- Armour, K. C., Marshall, J., Scott, J. R., Donohoe, A., & Newsom, E. R. (2016). Southern Ocean warming delayed by circumpolar upwelling and equatorward transport. *Nature Geoscience*, 9, 549–554. <https://doi.org/10.1038/NGEO2731>
- Bindoff, N. L., & McDougall, T. J. (1994). Diagnosing climate change and ocean ventilation using hydrographic data. *Journal of Physical Oceanography*, 24, 1137–1152. [https://doi.org/10.1175/1520-0485\(1994\)024<1137:DCCAOV>2.0.CO;2](https://doi.org/10.1175/1520-0485(1994)024<1137:DCCAOV>2.0.CO;2)
- Doddridge, E. W., Marshall, D. P., & Hogg, A. M. (2016). Eddy cancellation of the Ekman cell in subtropical gyres. *Journal of Physical Oceanography*, 46, 2995–3010. <https://doi.org/10.1175/JPO-D-16-0097.1>
- Farneti, R., & Delworth, T. L. (2010). The role of mesoscale eddies in the remote oceanic response to altered Southern Hemisphere winds. *Journal of Physical Oceanography*, 40, 2348–2354. <https://doi.org/10.1175/2010JPO4480.1>
- Farneti, R., Delworth, T. L., Rosati, A. J., Griffies, S. M., & Zeng, F. (2010). The role of mesoscale eddies in the rectification of the Southern Ocean response to climate change. *Journal of Physical Oceanography*, 40, 1539–1557. <https://doi.org/10.1175/2010JPO4353.1>
- Farneti, R., Downes, S. M., Griffies, S. M., Marsland, S. J., Behrens, E., Bentsen, M., et al. (2015). An assessment of Antarctic Circumpolar Current and Southern Ocean meridional overturning circulation during 1958–2007 in a suite of interannual CORE-II simulations. *Ocean Modelling*, 93, 84–120. <https://doi.org/10.1016/j.ocemod.2015.07.009>
- Frölicher, T. L., Sarmiento, J. L., Paynter, D. J., Dunne, J. P., Krasting, J. P., & Winton, M. (2015). Dominance of the Southern Ocean in anthropogenic carbon and heat uptake in CMIP5 models. *Journal of Climate*, 28, 862–886. <https://doi.org/10.1175/JCLI-D-14-00117.1>
- Gent, P. R. (2016). Effects of Southern Hemisphere wind changes on the meridional overturning circulation in ocean models. *Annual Review of Marine Science*, 8, 79–94. <https://doi.org/10.1146/annurev-marine-122414-033929>
- Gent, P. R., & Danabasoglu, G. (2011). Response to increasing Southern Hemisphere Winds in CCSM4. *Journal of Climate*, 24, 4992–4998. <https://doi.org/10.1175/JCLI-D-10-05011.1>
- Gent, P. R., & McWilliams, J. C. (1990). Isopycnal mixing in ocean circulation models. *Journal of Physical Oceanography*, 20, 150–155. [https://doi.org/10.1175/1520-0485\(1990\)020<0150:IMOCM>2.0.CO;2](https://doi.org/10.1175/1520-0485(1990)020<0150:IMOCM>2.0.CO;2)
- Gong, D., & Wang, S. (1999). Definition of Antarctic Oscillation Index. *Geophysical Research Letters*, 26, 459–462. <https://doi.org/10.1029/1999GL900003>
- Griffies, S. M., Gnanadesikan, A., Dixon, K. W., Dunne, J. P., Gerdes, R., Harrison, M. J., et al. (2005). Formulation of an ocean model for global climate simulations. *Ocean Science*, 1, 45–79. <https://doi.org/10.5194/os-1-45-2005>
- Hallberg, R. (2013). Using a resolution function to regulate parameterizations of oceanic mesoscale eddy effects. *Ocean Modelling*, 72, 92–103. <https://doi.org/10.1016/j.ocemod.2013.08.007>
- Hazel, J. E., & Stewart, A. L. (2019). Are the near-antarctic easterly winds weakening in response to enhancement of the southern annular mode? *Journal of Climate*, 32, 1895–1918. <https://doi.org/10.1175/JCLI-D-18-0402.1>
- Hofmann, M., & Morales-Maqueda, M. A. (2011). The response of Southern Ocean eddies to increased midlatitude westerlies: A non-eddy resolving model study. *Geophysical Research Letters*, 38, L03605. <https://doi.org/10.1029/2010GL045972>
- Kiss, A. E., Hogg, A. M., Hannah, N., Dias, F. B., Brassington, G. B., Chamberlain, M. A., et al. (2020). ACCESS-OM2: A global ocean-sea-ice model at three resolutions. *Geoscientific Model Development*, 13, 401–442. <https://doi.org/10.5194/gmd-13-401-2020>
- Kosempa, M., & Chambers, D. P. (2014). Southern Ocean velocity and geostrophic transport fields estimated by combining Jason altimetry and Argo data. *Journal of Geophysical Research: Oceans*, 119, 4761–4776. <https://doi.org/10.1002/2014JC009853>
- Li, Q., Lee, S., England, M. H., & McClean, J. L. (2019). Seasonal-to-interannual response of southern ocean mixed layer depth to the southern annular mode from a global $1/10^{\circ}$ ocean model. *Journal of Climate*, 32, 6177–6195. <https://doi.org/10.1175/JCLI-D-19-0159.1>
- Llovel, W., & Terray, L. (2016). Observed southern upper-ocean warming over 2005–2014 and associated mechanisms. *Environmental Research Letters*, 11, 124023. <https://doi.org/10.1088/1748-9326/11/12/124023>

- Locarnini, R. A., Mishonov, A. V., Antonov, J. I., Boyer, T. P., Garcia, H. E., Baranova, O. K., et al. (2013). World ocean atlas 2013, volume 1: Temperature. NOAA Atlas NESDIS, 73.
- Lovenduski, N. S., & Gruber, N. (2005). Impact of the Southern Annular Mode on Southern Ocean circulation and biology. *Geophysical Research Letters*, 32, L11603. <https://doi.org/10.1029/2005GL022727>
- Marshall, G. J. (2003). Trends in the Southern Annular Mode from observations and reanalyses. *Journal of Climate*, 16, 4134–4143. [https://doi.org/10.1175/1520-0442\(2003\)016<4134:TITSAM>2.0.CO;2](https://doi.org/10.1175/1520-0442(2003)016<4134:TITSAM>2.0.CO;2)
- Marshall, J., Scott, J. R., Armour, K. C., Campin, J.-M., Kelley, M., & Romanou, A. (2015). The ocean's role in the transient response of climate to abrupt greenhouse gas forcing. *Climate Dynamics*, 44, 2287–2299. <https://doi.org/10.1007/s00382-014-2308-0>
- Redi, M. H. (1982). Oceanic isopycnal mixing by coordinate rotation. *Journal of Physical Oceanography*, 12, 1154–1158. [https://doi.org/10.1175/1520-0485\(1982\)012<1154:OIMBCR>2.0.CO;2](https://doi.org/10.1175/1520-0485(1982)012<1154:OIMBCR>2.0.CO;2)
- Roemmich, D., Church, J., Gilson, J., Monselesan, D., Sutton, P., & Wijffels, S. (2015). Unabated planetary warming and its ocean structure since 2006. *Nature Climate Change*, 5, 240–245. <https://doi.org/10.1038/nclimate2513>
- Sallée, J. B., Speer, K. G., & Rintoul, S. R. (2010). Zonally asymmetric response of the Southern Ocean mixed-layer depth to the Southern Annular Mode. *Nature Geoscience*, 3, 273–279. <https://doi.org/10.1038/NGEO812>
- Sen Gupta, A., & England, M. H. (2006). Coupled ocean-atmosphere-ice response to variations in the Southern Annular mode. *Journal of Climate*, 19, 4457–4485. <https://doi.org/10.1175/JCLI3843.1>
- Spence, P., Griffies, S. M., England, M. H., Hogg, A. M., Saenko, O. A., & Jourdain, N. C. (2014). Rapid subsurface warming and circulation changes of Antarctic coastal waters by poleward shifting winds. *Geophysical Research Letters*, 41, 4601–4610. <https://doi.org/10.1002/2014GL060613>
- Stewart, K. D., Hogg, A. M., Griffies, S. M., Heerdegen, A. P., Ward, M. L., Spence, P., & England, M. H. (2017). Vertical resolution of baroclinic modes in global ocean models. *Ocean Modelling*, 113, 50–65. <https://doi.org/10.1016/j.ocemod.2017.03.012>
- Stewart, K. D., Kim, W. M., Urakawa, S., Hogg, A. M., Yeager, S., Tsujino, H., et al. (2020). JRA55-do-based repeat year forcing datasets for driving ocean-sea-ice models. *Ocean Modelling*, 147, 101557. <https://doi.org/10.1016/j.ocemod.2019.101557>
- Thompson, D. W. J., & Solomon, S. (2002). Interpretation of recent Southern Hemisphere climate change. *Science*, 296, 895–899. <https://doi.org/10.1126/science.1069270>
- Thompson, D. W. J., & Wallace, J. M. (2000). Annular modes in the extratropical circulation. Part I: Month-to-month variability. *Journal of Climate*, 13, 1000–1016. [https://doi.org/10.1175/1520-0442\(2000\)013<1000:AMITEC>2.0.CO;2](https://doi.org/10.1175/1520-0442(2000)013<1000:AMITEC>2.0.CO;2)
- Thompson, D. W. J., Wallace, J. M., & Hegerl, G. C. (2000). Annular modes in the extratropical circulation. Part II: Trends. *Journal of Climate*, 13, 1018–1036. [https://doi.org/10.1175/1520-0442\(2000\)013<1018:AMITEC>2.0.CO;2](https://doi.org/10.1175/1520-0442(2000)013<1018:AMITEC>2.0.CO;2)
- Treguier, A. M., Sommer, J. L., Molines, J. M., & Cuevas, B. (2010). Response of the Southern Ocean to the Southern Annular Mode: Interannual variability and multidecadal trend. *Journal of Physical Oceanography*, 40, 1659–1668. <https://doi.org/10.1175/2010JPO4364.1>
- Tsujino, H., Urakawa, S., Nakano, H., Small, R. J., Kim, W. M., Yeager, S. G., et al. (2018). JRA-55 based surface dataset for driving ocean-sea-ice models (JRA55-do). *Ocean Modelling*, 130, 79–139. <https://doi.org/10.1016/j.ocemod.2018.07.002>
- Waugh, D. W., & Haine, T. W. N. (2020). How rapidly do the southern subtropical oceans respond to wind stress changes? *Journal of Geophysical Research: Oceans*, 125, e2020JC016236. <https://doi.org/10.1029/2020JC016236>
- Waugh, D. W., Hogg, A. M., Spence, P., England, M. H., & Haine, T. W. N. (2019). Response of Southern Ocean ventilation to changes in midlatitudes westerly winds. *Journal of Climate*, 32, 5345–5361. <https://doi.org/10.1175/JCLI-D-19-0039.1>
- Zheng, F., Li, J., Clark, R. T., & Nnamchi, H. C. (2013). Simulation and projection of the Southern Hemisphere Annular Mode in CMIP5 Models. *Journal of Climate*, 26, 9860–9879. <https://doi.org/10.1175/JCLI-D-13-00204.1>
- Zika, J. D., England, M. H., & Sijp, W. P. (2012). The ocean circulation in thermohaline coordinates. *Journal of Physical Oceanography*, 42, 708–724. <https://doi.org/10.1175/JPO-D-11-0139.1>
- Zweng, M. M., Reagan, J. R., Antonov, J. I., Locarnini, R. A., Mishonov, A. V., Boyer, T. P., et al. (2013). World Ocean Atlas 2013, volume 2: Salinity. NOAA Atlas NESDIS, 74.